AIAA JOURNAL
Vol. 39, No. 6, June 2001

Technical Notes

TECHNICAL NOTES are short manuscripts describing new developments or important results of a preliminary nature. These Notes cannot exceed six manuscript pages and three figures; a page of text may be substituted for a figure and vice versa. After informal review by the editors, they may be published within a few months of the date of receipt. Style requirements are the same as for regular contributions (see inside back cover).

Double Flutter in an Aeroelastic System

Pavel A. Chamara* and B. D. Coller†
University of Illinois at Chicago, Chicago, Illinois 60607-7022

Nomenclature

b_j = semichord of jth airfoil
$\tilde{d}$ = dimensionless blade spacing
$\tilde{h}_j$ = dimensionless plunge (positive upward), h_j/b_j
$\tilde{L}_j$ = dimensionless lift, $L_j/\pi\rho b_j U^2$
$\tilde{M}_{\mathrm{ea}_j}$ = dimensionless moment about elastic axis, $M_{ea_j}/\pi\rho b_j^2 U^2$
r_{α_j} = dimensionless radius of gyration, $I_{\mathrm{ea}_j}/m_j b_j^2$
$\tilde{U}$ = dimensionless flow speed, $U/b_1\omega_{\alpha_1}$
$\tilde{W}$ = dimensionless blade upwash, W/U
X_j = frequency ratio, $\omega_{h_j}/\omega_{\alpha_j}$
Y_j = interblade frequency ratio, $\omega_{\alpha_j}/\omega_{\alpha_1}$
α_j = airfoil pitch (positive nose up)
β_j = airfoil size ratio, b_j/b_1
μ_j = mass ratio, $m_j/\pi\rho b_j^2$
τ = dimensionless time, $\omega_{\alpha_1} t$
χ_j = dimensionless static unbalance

I. Introduction

We consider two airfoils elastically suspended in a two-dimensional, nominally uniform flow of an inviscid and incompressible fluid. Each airfoil has two degrees of freedom, pitch and plunge, and the dynamics of the two blades are coupled aerodynamically through the fluid, but not structurally. An illustration with several physical parameters is presented in Fig. 1.

As with the single-airfoil problem, there exists a critical flutter speed U_F, above which the system exhibits an aeroelastic instability known as flutter. Here, we are interested in configurations of the two-airfoil system for which two oscillatory instabilities occur simultaneously: double flutter. Mathematically speaking, if we were to linearize the dynamics and calculate the spectrum, the situation would correspond to two conjugate pairs of complex eigenvalues crossing the imaginary axis simultaneously as the flow speed U increases past U_F, the flutter speed. Such conditions have been shown to exist in a single airfoil with control surface,[1] as well as in plates and shells.[2]

In the jargon of nonlinear dynamic systems theory, such a situation is called a codimension two Hopf–Hopf bifurcation. In addition to our simple curiosity, we are interested in the problem because of the very rich nonlinear dynamics that often arise from such instabilities.[3] Nonlinear phenomena may include small-amplitude periodic and quasi-periodic orbits that can be exploited for making passive flow control actuators.

Received 3 October 2000; revision received 1 March 2001; accepted for publication 8 March 2001.

*Graduate Student, Department of Mechanical Engineering, 842 W. Taylor Street.
†Assistant Professor, Department of Mechanical Engineering, 842 W. Taylor Street. Member AIAA.

One may trivially create a Hopf–Hopf bifurcation by choosing the distance $\tilde{d}$ between airfoils sufficiently large so that the two blades are essentially uncoupled. With independent blade dynamics in such cases, it is a simple matter to choose physical parameters so that both have the same flutter velocity. Motivated by the possibility of rich nonlinear dynamic interaction between the blades, however, we seek double flutter in systems with strong coupling.

II. Modeling

The linearized equations of motion for the airfoils in the two-blade cascade are given by

$$\tilde{h}_j'' - \chi_j\alpha_j'' + X_j^2 Y_j^2 \tilde{h}_j = \left(\tilde{U}^2/\mu_j\beta_j^2\right)\tilde{L}_j$$
$$-\chi_j\tilde{h}_j'' + r_{\alpha_j}^2\alpha_j'' + r_{\alpha_j}^2 Y_j^2\alpha_j = \left(\tilde{U}^2/\mu_j\beta_j^2\right)\tilde{M}_{\mathrm{ea}_j} \qquad (1)$$

where the index j refers to the jth blade and prime denotes differentiation with respect to dimensionless time τ. To represent the linear aerodynamic lifts and moments, we utilize two models. The first is a relatively high-fidelity vortex lattice simulation, similar to those of Refs. 4 and 5, in which the wakes behind each airfoil are assumed to lie in the nominal planes of the airfoils. The aerodynamic loading, induced on one airfoil by the motion of the other, is included in the model.

A second, low-order model, amenable to timely analysis for a variety of system parameters, is derived from the high-fidelity simulation. In developing the low-order model, we take an approach similar to Ref. 6, envisioning the aeroelastic problem as a general gray-box input/output system: the inputs are the blade motions, and the outputs are aerodynamic lifts and moments. As in the case of a single airfoil, we write aerodynamic forces such as lift as a sum of two different types of terms: $\tilde{L}_j = \tilde{L}_j^{(M)} + \tilde{L}_j^{(C)}$. The superscript (M) denotes a set of memoryless terms, mostly of apparent mass origin, that are linear functions of accelerations. The (C) superscript refers to terms that tend to be of circulatory type. For a single airfoil, Fung[7] writes this latter part as a Duhamel integral, which convolves Wagner's function Φ with $\tilde{W}_{3/4}^{(m)\prime}$, the time derivative of the upwash at the three-quarter chord location due to blade motion.

In the two-airfoil problem, we mold the aerodynamic response into a similar formulation. Because we know of no privileged

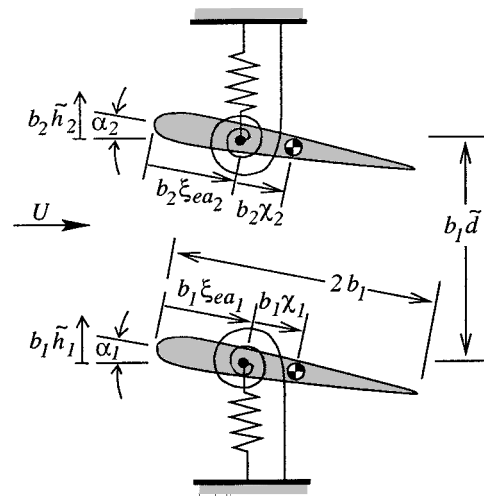

Fig. 1 System of two airfoils.

location such as the three-quarter chord point in the single-airfoil problem that conveys all of the necessary information, we must consider the distribution of upwash over the entire blades. However, for flat blades, the upwash on the jth blade induced by its motion must be spatially linear:

$$\tilde{W}_j^{(m)}(\xi,\tau) = W_j^{(m)}/U = -(\beta_j/\tilde{U})\tilde{h}_j' + \alpha_j + (\beta_j/\tilde{U})(\xi - \xi_{\mathrm{ea}})\alpha_j'$$
$$= p_j(\tau)\tilde{W}_{U_j}(\xi) + q_j(\tau)\tilde{W}_{R_j}(\xi)$$

In the last equality, we decompose the linear upwash into spatially uniform, $\tilde{W}_{U_j}(\xi)=1$, and spatially ramplike, $\tilde{W}_{R_j}(\xi)=\xi$, components, respectively, with expansion coefficients $p_j = -\tilde{h}_j'\beta_j/\tilde{U} + \alpha_j - \xi_{\mathrm{ea}_j}\alpha_j'\beta_j/\tilde{U}$ and $q_j = \alpha_j'\beta_j/\tilde{U}$. Therefore, to model the circulatory part of the lift on one of the blades, we employ four Duhamel integrals:

$$\tilde{L}_j^{(C)} = \int_{-\infty}^{\tau} \Phi_{U_{j1}}[\tilde{U}(\tau-\tau_0)]\frac{\mathrm{d}\tilde{W}_{U_1}}{\mathrm{d}\tau_0}\,\mathrm{d}\tau_0 + \int_{-\infty}^{\tau} \Phi_{U_{j2}}[\tilde{U}(\tau-\tau_0)]\frac{\mathrm{d}\tilde{W}_{U_2}}{\mathrm{d}\tau_0}\,\mathrm{d}\tau_0 + \int_{-\infty}^{\tau} \Phi_{R_{j1}}[\tilde{U}(\tau-\tau_0)]\frac{\mathrm{d}\tilde{W}_{R_1}}{\mathrm{d}\tau_0}\,\mathrm{d}\tau_0 + \int_{-\infty}^{\tau} \Phi_{R_{j2}}[\tilde{U}(\tau-\tau_0)]\frac{\mathrm{d}\tilde{W}_{R_2}}{\mathrm{d}\tau_0}\,\mathrm{d}\tau_0 \quad (2)$$

that incorporate the spatially uniform and ramplike upwash inputs of both blades. The analogs Φ_* to Wagner's function may be determined numerically from our high-fidelity model by individually simulating step responses to the four inputs: W_{U_1}, W_{U_2}, W_{R_1} and W_{R_2}.

To incorporate these effects into a low-order model, we fit the step response simulation data with exponentials:

$$\Phi_*(\tau) \approx \phi_{*\infty}\left(1 - \sum_{m=1}^{N_*} K_{*m} e^{\sigma_{*m}\tau}\right) \quad (3)$$

Following the procedure outlined in Ref. 8, we can then reexpress the integral

$$\int_{-\infty}^{\tau} \Phi_*(\tau-\tau_0)\frac{\mathrm{d}\tilde{W}_*}{\mathrm{d}\tau_0}\,\mathrm{d}\tau_0 \approx G_{*0}(\tau) + G_{*1}(\tau) + \cdots + G_{*N_*}(\tau) \quad (4)$$

where

$$G_{*0}(\tau) = \phi_{*\infty}\left(1 - \sum_{m=1}^{N_*} K_{*m}\right)\tilde{W}_*(\tau)$$

$$G_{*m}'(\tau) = \sigma_{*m}\tilde{U}[G_{*m}(\tau) - \phi_{*\infty}K_{*m}\tilde{W}_*(\tau)]$$

Thus, the circulatory parts of the system are expressed as a combination of simple linear ordinary differential equations.

Because the memoryless terms tend to represent apparent mass effects proportional to blade acceleration, we express them in terms of time derivatives of upwash inputs:

$$\tilde{L}_j^{(M)} = \left(C_{U_{j1}}/\tilde{U}\right)\tilde{W}_{U_1}' + \left(C_{U_{j2}}/\tilde{U}\right)\tilde{W}_{U_2}' + \left(C_{R_{j1}}/\tilde{U}\right)\tilde{W}_{R_1}' + \left(C_{R_{j2}}/\tilde{U}\right)\tilde{W}_{R_2}'$$

The coefficients C_* are determined by the high-fidelity simulation being run with the input upwash modes individually varying sinusoidally in time. After the subtraction of the circulatory part of the lift from the numerical lift data, it is a simple matter to fit the coefficients. The procedure yields the same coefficients regardless of the chosen forcing frequency.

On substitution of the lift model into Eq. (1), we arrive at a low-order linear model for the dynamic system. In standard state-space representation, it can be written as $\boldsymbol{x}' = B\boldsymbol{x}$, where the vector $\boldsymbol{x}$ contains all coordinates for the two airfoils, their time derivatives, and the G_{*m} fluid quantities such as those that appear in Eq. (4).

In Fig. 2, we plot the flutter boundary as a function of the frequency ratio X_2. Other parameters that are held fixed are $\chi_1 = 0.1$, $X_1 = 2$, $\mu_1 = 20$, $\xi_{\mathrm{ea}_1} = 0.5$, $r_{\alpha_1} = 0.5$, $\chi_2 = 0.2$, $\mu_2 = 20$, $\xi_{\mathrm{ea}_2} = 0.1$, $r_{\alpha_2} = 0.5$, $Y_2 = 2.0$, $\tilde{d} = 0.5$ and $\beta_2 = 1$. The solid curve represents the boundary predicted by the low-order models, whereas the circular symbols indicate flutter velocities exhibited by the high-fidelity simulation.

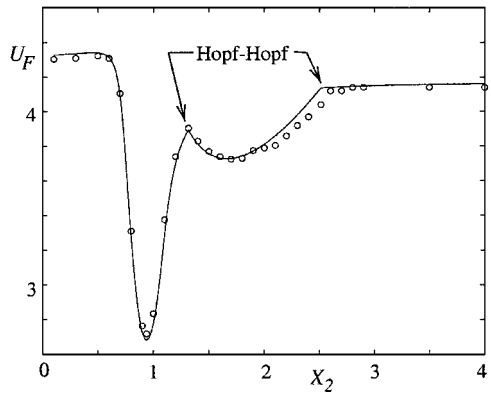

Fig. 2 Comparison of flutter boundary for high-fidelity simulation (symbols) to that predicted by the low-order model (solid).

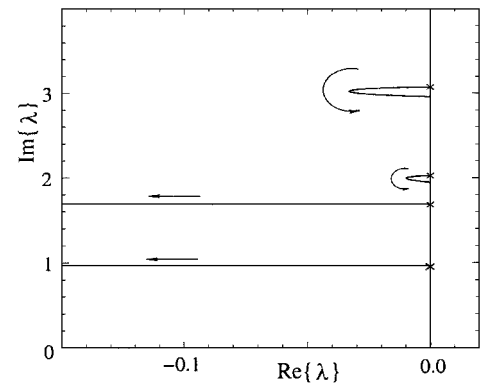

Fig. 3 Loci of real and imaginary parts of oscillatory eigenvalues for $X_2 = 1.315$ and $\tilde{U}$ increasing from zero to $\tilde{U}_F$.

III. Results

We observe that the flutter curve shown in Fig. 2 exhibits an abrupt change in character at $X_2 = 1.315$. For X_2 slightly less than this value, the instability occurs in a mode for which the relative magnitudes of the state variables are $(|h_1|, |\alpha_1|, |h_2|, |\alpha_2|) = (1.0, 0.540, 0.042, 0.189)$. For X_2 slightly greater, the critical mode has relative magnitudes $(|h_1|, |\alpha_1|, |h_2|, |\alpha_2|) = (0.111, 0.072, 0.796, 1.0)$. At $X_2 = 1.315$, both modes lose stability simultaneously, and we encounter the Hopf–Hopf bifurcation we sought to find. Part of the root locus plot for the Hopf–Hopf case is shown in Fig. 3 as $\tilde{U}$ varies from zero to $\tilde{U}_F = 3.894$. The eigenvalues shown are those that lie on the positive imaginary axis when $\tilde{U} = 0$. The complex conjugates of those shown are also eigenvalues. We see clearly that two pairs of eigenvalues cross the imaginary axis at $\tilde{U} = \tilde{U}_F$.

Inspection of the lightly damped modes clearly shows strong dynamic coupling between the blades. Further evidence of strong dynamic coupling appears in Fig. 2 because variations in the frequency ratio X_2 of blade 2 has a significant effect on the flutter speed of a mode that mostly involves blade 1. Thus, the Hopf–Hopf bifurcation we detect here clearly involves the interaction among linear modes, providing a nontrivial example of the Hopf–Hopf instability. Preliminary investigation of the linear system indicates that the double Hopf bifurcation is by no means a rare phenomenon and can be found for a wide range of system parameters. In fact, a second double Hopf bifurcation is apparent in Fig. 2 at $X_2 = 2.51$, where the flutter curve changes abruptly again.

IV. Conclusions

Given the existence of Hopf–Hopf instabilities we have encountered in such aeroelastic systems, we are now motivated to engage

in nonlinear analysis, to unfold the potentially rich dynamics associated with double flutter, and to explore opportunities to utilize the instability for beneficial purposes.

Acknowledgment

We appreciate helpful comments from Earl H. Dowell.

References

[1]Tang, D. M., Dowell, E. H., and Virgin, L., "Limit Cycle Behavior of an Airfoil with a Control Surface," *Journal of Fluids and Structures*, Vol. 12, No. 7, 1998, pp. 839–858.

[2]Dowell, E. H., *Aeroelasticity of Plates and Shell*, Kluwer, Dordrecht, The Netherlands, 1975, p. 63.

[3]Coller, B. D., "Surge/Stall Interactions in Compressors. Part I: Theoretical Development," Dynamical Systems and Control Lab., Technical Rept. DSCL 00–01, Univ. of Illinois, Chicago, 2000.

[4]Kim, M. J., and Mook, D. T., "Application of Continuous Vorticity Panels to General Unsteady Incompressible Two-Dimensional Lifting Flows," *Journal of Aircraft*, Vol. 23, No. 6, 1986, pp. 464–471.

[5]Hall, K. C., "Eigenanalysis of Unsteady Flows, about Airfoils, Cascades, and Wings," *AIAA Journal*, Vol. 32, No. 12, 1994, pp. 2426–2432.

[6]Dat, R., Tran, C. T., and Petot, D., "Semi-Empirical Model for the Dynamic Stall of Airfoils in View of the Application to the Calculation of Responses of a Helicopter Blade in Forward Flight," *Vertica*, Vol. 5, No. 1, 1981, pp. 35–53.

[7]Fung, Y. C., *An Introduction to the Theory of Aeroelasticity*, Dover, New York, 1993, pp. 206–210.

[8]Coller, B. D., and Chamara, P. A., "Structural Nonlinearities and the Nature of the Classic Flutter Instability," Dynamical Systems and Control Lab., Technical Rept. DSCL 00–03, Univ. of Illinois, Chicago, 2000.

E. Livne
Associate Editor

Numerical Computations of Purely Radial Flow Within Two Concentric Disks

Wahid S. Ghaly* and Georgios H. Vatistas†
Concordia University, Montreal, Quebec H3G 1M8, Canada

Introduction

THE radial flow within the gap formed by placing two flat disks together is pertinent to a number of engineering applications, such as radial diffusers, air-bearing, disk-type heat exchangers, pneumatic micrometers, and several others. Two distinct types of flow can evolve within such domains. The accelerating (or sink) flow is produced by admitting the fluid through the periphery and draining it from a centrally located outlet. This type of fluid motion is characterized by a monotonically decreasing pressure gradient. Because of the stabilizing effects of acceleration, it is also known to remain laminar even at very high Reynolds numbers or to laminarize in the case where the entering fluid is initially turbulent.[1] Decelerating (or source) flow emerges by introducing the fluid into the domain through a centrally located inlet. Mochizuki and Yang[2] reported on three distinct manifestations of such fluid motion. At low inlet Reynolds numbers, they observed a steady, laminar, unidirectional flow throughout the gap. For intermediate inlet Reynolds numbers, a decaying self controlled oscillatory flow appeared. Finally, for high inlet Reynolds numbers, a self-sustained fluctuating flow, evolving into a laminar–turbulent transition, followed by a reverse flow transformation to laminarlike conditions at larger radii was evident. In many respects, the disk flows are similar to the classical Jeffery–Hammel flows between two inclined planes.

The present Note reports on the numerical solution of purely radial converging and diverging flows between two stationary disks. Assuming a unidirectional flow, continuity and momentum equations are reduced into a third-order ordinary differential equation (ODE) involving only the radial velocity. The solution of the latter nonlinear equation is accomplished using a variation of the shooting method, developed by Keller in Ref. 3, where the governing equation is written as a system of three nonlinear first order ODEs, and the resulting system is solved as an initial value problem via the fourth-order Runge–Kutta method. The same method has been used previously by the authors to study the flow development in spherical and conical passages.[4,5] This numerical method is simple and fast compared with the conventional use of computational fluid dynamics (CFD) in solving fluid flow problems. The results obtained are compared with some available experimental data for the velocity and pressure in accelerating and decelerating flows.

Problem Formulation and Solution Technique

Consider the steady, laminar, incompressible, nonswirling, purely radial flow developed in the gap between a pair of parallel disks that is shown schematically in Fig. 1. From Ref. 6, the equations describing this type of fluid motion are as follows.

Continuity:

$$\int_0^1 g(\zeta)\,\mathrm{d}\zeta = \pm 1 \tag{1}$$

Radial momentum:

$$g''(\zeta) + \lambda^2 g^2(\zeta) = \lambda^2 \Delta\Pi \tag{2}$$

where g'' indicates the second derivative of g with respect to ζ,

$$\lambda^2 = \frac{(r^2-1)Re_r}{2r^2\,\ell n(r)}, \qquad \Delta\Pi = \frac{2r^2\Delta P}{r^2-1}$$

$V_r r = g(\zeta)$, where $r = r^*/R_0^*$, $\zeta = z^*/h^*$, $V_r = V_r^*/V_0^*$, V_r^* is the radial velocity component, and V_0^* is the average velocity at R_0^*, and $Re = \rho^* V_0^* h^*/\mu^*$, $Re_r = Re\,\xi$, $\xi = h^*/R_0^*$, $\Delta P = (P^* - P_0^*)/\rho^* V_0^{*2}$, where p^* is the static pressure at r^*, P_0^* is the static pressure at R_0^*, and ρ and μ are the fluid density and viscosity, respectively. The asterisks indicate a dimensional quantity, the plus and minus signs in the continuity equation represent outflow and inflow, respectively, and the rest of the parameters used are defined in Fig. 1.

On differentiation of Eq. (1) with respect to ζ,

$$g'''(\zeta) + \lambda^2 g(\zeta) g'(\zeta) = 0 \tag{3}$$

The required boundary conditions are

$$\zeta = 0 \;\rightarrow\; \frac{\mathrm{d}g(\zeta)}{\mathrm{d}\zeta} = 0 \tag{4a}$$

$$\zeta = 1 \;\rightarrow\; g(\zeta) = 0 \tag{4b}$$

The two conditions given correspond to the nonslip condition of the velocity at the plates and the symmetrical nature of the velocity

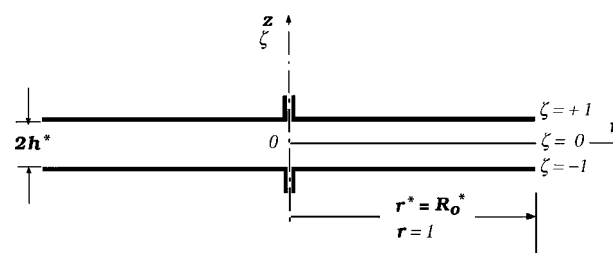

Fig. 1 Schematic of problem.

Received 15 March 2000; revision received 11 October 2000; accepted for publication 21 December 2000.

*Associate Professor, Department of Mechanical Engineering. Senior Member AIAA.

†Professor, Department of Mechanical Engineering. Senior Member AIAA.